High Depolarization Ratios of Naturally Occurring Cirrus Clouds Near Air Traffic Regions Over Europe

Benedikt Urbanek[1] (iD), Silke Groß[1] (iD), Martin Wirth[1], Christian Rolf[2] (iD), Martina Krämer[2] (iD), and Christiane Voigt[1] (iD)

[1]Institut für Physik der Atmosphäre, Deutsches Zentrum für Luft- und Raumfahrt e.V, Oberpfaffenhofen, Germany, [2]Institut für Energie- und Klimaforschung (IEK-7), Forschungszentrum Jülich GmbH, Jülich, Germany

Abstract Cirrus clouds have a large influence on the Earth's climate and anthropogenic activities such as aviation can alter their properties. Besides the formation of contrails, indirect effects on naturally occurring cirrus like increased heterogeneous freezing due to exhaust soot particles are discussed in the literature. However, hardly any observational study exists. In this work we present cirrus optical properties measured by an airborne lidar over Europe during the Midlatitude Cirrus experiment (ML-CIRRUS). One half of the cloud cases showed elevated depolarization ratios with a mode difference of 10 percentage points indicating differences in the clouds microphysical properties. Their origin can be traced back to highly frequented air traffic regions, and they show lower in-cloud ice supersaturations. Our analysis reveals no influence of embedded contrails and temperature. These results could be explained by an indirect aerosol effect where heterogeneous freezing is caused by aviation exhaust particles.

Plain Language Summary Civil airplanes emit exhaust gases and soot into the atmosphere, which can influence the Earth's climate in several ways. One possibility could be that emitted soot particles alter the formation of ice clouds, which has a potentially high climate impact. However, observational studies of this process are sparse. In this work we present ice clouds measured above Europe by an airborne remote sensing instrument. One group of clouds features elevated depolarization ratios implying altered crystal habits. It also shows lower ice supersaturation indicating a modified ice formation. We demonstrate that this is not caused by condensation trails present inside the clouds, by temperature, or by the dynamical state of the atmosphere. However, these clouds had formed in air that stemmed from highly frequented aviation corridors. Thus, our observations could be the first traces of this indirect process.

1. Introduction

Global mobility is gaining an increasing importance in human society. As a consequence, air traffic volume showed annual growth rates of more than 4% in the last years and is predicted to do so in the coming decades (ICAO "Long-Term Traffic Forecasts" 2016). This leaves geosciences with the urgent task to quantify the numerous aviation impacts on climate (Lee et al., 2009).

Radiative forcing (RF) results from direct engine emissions in the upper troposphere (Lund et al., 2017) and from contrails that form under suitable conditions (Burkhardt et al., 2010). In the last years, a lot of research effort has been dedicated to measuring and understanding contrails (Heymsfield et al., 2010; Iwabuchi et al., 2012; Kärcher et al., 2015; Schumann et al., 2017; Voigt et al., 2011) and to determining the climatic effect that arises from their increasing occurrence (Burkhardt & Kärcher, 2011).

Contrails also alter the properties of cirrus clouds. Tesche et al. (2016) studied contrail formation in preexisting cirrus. They analyzed satellite lidar measurements and could show that embedded contrails cause an increase in cloud optical thickness inside individual flight tracks compared to adjacent parts of the cloud.

The total RF from contrails is small compared to that of natural ice clouds. Therefore, indirect aviation effects that alter the properties of natural cirrus can potentially have a high climatic impact. Jensen and Toon (1997) suggested already two decades ago that aircraft exhaust particles may act as efficient ice nuclei leading to more heterogeneous freezing in polluted regions.

A number of modeling studies simulated this indirect aerosol effect (Gettelman & Chen, 2013; Hendricks et al., 2005; Kärcher et al., 2007; Zhou & Penner, 2014).Their estimations of the radiative impact provide

contradicting results that range from no statistical effect to a range between -0.35 and 0.09 Wm^{-2} (Gettelman & Chen, 2013; Zhou & Penner, 2014). These studies suffer from huge uncertainties that stem from a lack of in situ observations that could help restrict model scenarios. Still, this effect may potentially alter cirrus properties in large areas of the globe and therefore could cause RF that exceeds that of contrails.

To our knowledge, only two field campaign studies tried to investigate this indirect effect. Ström and Ohlsson (1998) examined airborne in situ measurements and found increased ice crystal number densities in confined regions inside cirrus clouds that also showed elevated black carbon concentrations. This was confirmed by Kristensson et al. (2000). They found reduced effective ice diameters and therefore increased number densities during the same campaign. However, it remains unclear whether their observations were caused by heterogeneous nucleation on exhaust particles, as they could also be interpreted as the direct effect of embedded contrails on cirrus clouds.

In our work, we present cirrus particle linear depolarization ratios (PLDRs) measured with an airborne high-spectral-resolution lidar during the ML-CIRRUS campaign 2014 over Europe. PLDR is a well-defined optical property that can be used to retrieve information on ice habit from lidar measurements (Del Guasta et al., 1998; Noel et al., 2002; Schnaiter et al., 2012). When linearly polarized light is scattered by atmospheric ice crystals, reflections at internal facets can lead to skew ray paths that result in a change of polarization. The strength of this effect can be evaluated by analyzing the backscattered light, splitting it into the polarization components perpendicular and parallel to the incident light. PLDR is defined as the power ratio of both components and therefore mainly determined by the precise crystal shape.

Columnar ice crystals, often found at higher altitudes, are expected to show higher PLDR than plate-like crystals that are more dominant at lower altitudes (Noel et al., 2006). However, multiple crystal habits could lead to the same PLDR. A satellite-based study determined a global averaged depolarization ratio of 35% (Sassen & Zhu, 2009). In the clouds investigated during the ML-CIRRUS campaign, we find a strong bimodal PLDR distribution with a mode difference of about 10 percentage points and analyze this shift in the context of a possible indirect aerosol effect from aviation.

2. Methods

In spring 2014, the ML-CIRRUS campaign was conducted with the goal to study cirrus properties in meteorological regimes typical for midlatitudes, to observe contrail cirrus, and to investigate differences between anthropogenic and natural cirrus. For this, the German High Altitude and Long Range Research Aircraft (HALO) was equipped with a combined in situ and remote sensing instrumentation (Voigt et al., 2017). Flight planning was guided by meteorological forecasts and advanced model predictions of cirrus and contrails (Schumann, 2012; Schumann & Graf, 2013). The flights cover the whole range of the midlatitudes from 35°N to 60°N and from the Atlantic Ocean (14°W) to central Europe (14°E). More details on the flights, instrumentation, flight planning, and forecast products can be found in Voigt et al. (2017, their Table 3).

The high-spectral-resolution and differential absorption lidar WALES (derived from WAter vapor Lidar Experiment in Space) aboard HALO is capable of measuring backscatter ratio (BSR) at 532 and 1,064 nm, PLDR at 532 nm, and water vapor (WV) concentration, with a high vertical resolution. A definition of PLDR and a description of the system can be found in Esselborn et al. (2008), PLDR is their $\delta_a(r)$, and Wirth et al. (2009). For determining PLDR, we employed an advanced, two-angle $\pm45°$ calibration scheme (Freudenthaler et al., 2009), achieving an absolute accuracy of 5 percentage points at typical cirrus PLDR values.

In order to exclude liquid and mixed phase clouds and aerosol layers from the data, we only consider measurements at temperatures below 235 K and above a BSR threshold of 3, respectively. The BSR threshold was determined after carefully inspecting all flight legs for aerosol layers, and we found our further analysis to be only weakly dependent on the exact choice of BSR threshold within the range from 2 to 25.

From measured WV and model temperature (6-hourly analysis data from ECMWF (European Centre for Medium-Range Weather Forecasts)), we determine RH_i using the parameterization for WV saturation by Murphy and Koop (2005). This approach was demonstrated and validated by Groß et al. (2014). Calculating RHi inside of cirrus from model temperature could potentially lead to inaccuracies, as temperature fluctuations might not be properly resolved. However, the resulting RHi distributions feature the same positively skewed shape that was also found in in situ measurements of cold cirrus clouds,
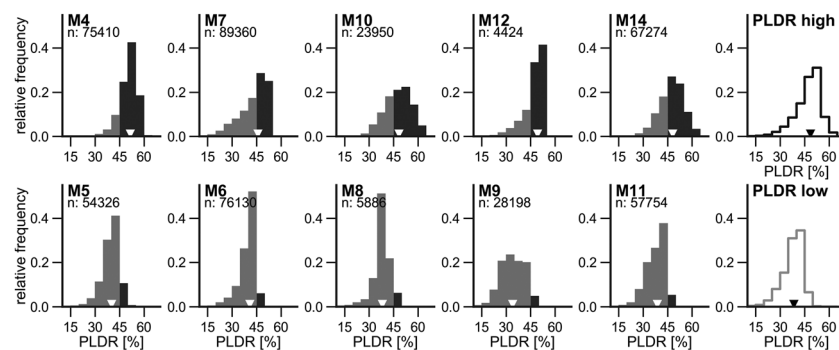
Figure 1. Histogram of particle linear depolarization ratios (PLDRs) inside ice clouds (BSR > 3, T < 235 K) for 10 mission flights and averaged histograms of the upper row (PLDR high) and lower row (PLDR low). Values above 45% are highlighted in black, medians are marked by a triangle, and n gives the number of lidar data points. BSR = backscatter ratio.

for example, during the INCA campaign and the MOZAIC project (Ovarlez et al., 2002; Spichtinger et al., 2004). Therefore, we are confident that this method is well suited for our analysis.

We also consider the origin of the air masses the clouds formed in, by examining 24-hr backward trajectories. They are calculated on horizontal wind data (ECMWF reanalysis Era-Interim, 1° by 1° resolution) using diabatic heating rates for vertical transport with the trajectory module of CLaMS (McKenna et al., 2002). The starting points of these trajectories are distributed over the lidar cross section with a temporal resolution of 12 s (about 2.4 km) and a vertical resolution of 150 m. The cloud ice water content (IWC) is interpolated from the reanalysis onto the trajectory paths.

3. Observations

During 10 campaign missions, cirrus clouds were measured by lidar. The mission flights took place on different days and in different air masses; therefore, these observations can be seen as statistically independent from each other. The measured vertical cloud cross sections range from 73 km^2 (M12) to 1477 km^2 (M7).

Looking at the PLDR distributions inside these clouds, two groups can be identified (Figure 1). The distributions in the upper row (M4, M7, M10, M12, and M14) show significantly higher PLDR than distributions in the lower row, with values up to 65% and modes and medians above 45%. Most of the upper row distributions also show very little depolarization below 30%. In the lower row (M5, M6, M8, M9, and M11), distributions show sharp cutoffs above 45% with modes below 45% and medians below 41%. Most of them have considerable cloud fractions with depolarizations below 30%. We refer to these two groups as "PLDR high" and "PLDR low." The two distributions on the right are the averages over the five distributions to the left in each row. They form two separate modes with a mode difference of 10%. Their medians (means) are located at 38.4% (37.5%) and 48.7% (47.2%), and they have standard deviations of 6.3% and 7.2%, respectively.

We investigate the temperature dependence of PLDR by calculating the median of PLDR measurements in 1-K temperature bins for every mission (Figure 2a). PLDR high and PLDR low cases show a negative trend with lower PLDR at higher temperatures. This is a well-known feature of cirrus clouds that is typically explained by the dominance of different ice shapes at different temperatures (columnar particles at higher altitudes and plate-like particles at lower altitudes; Del Guasta & Vallar, 2003; Sassen & Benson, 2001; Um et al., 2015). However, we find an offset in PLDR between the two groups in the entire temperature range from 235 to 207 K.

In Figure 2b, we plot the histogram of RH$_i$ inside PLDR high and PLDR low clouds. They are calculated by averaging over five normalized distributions for each group. This ensures that the resulting histogram is weighted by the number of independent observations rather than by the cross section of the clouds. PLDR high clouds reach lower supersaturations and have a supersaturated fraction of 30%, whereas clouds in PLDR low have a supersaturated fraction of 41%. We verified the significance of this finding by employing a statistical resampling method: When randomly choosing two groups of five cases each, from the 10 observations and calculating their RH$_i$ distributions as in Figure 2b, the probability to
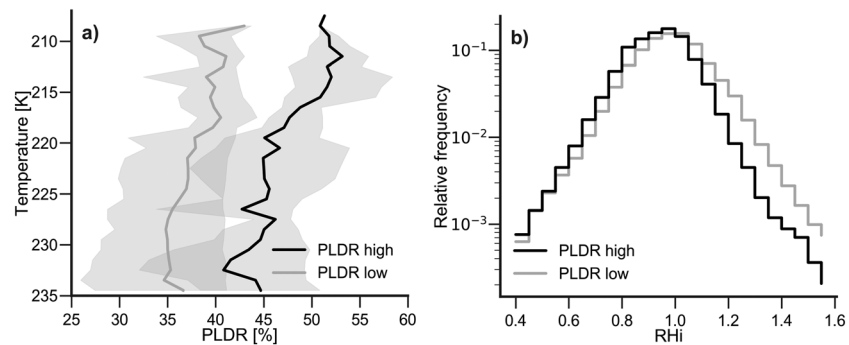
Figure 2. (a) Temperature dependence of particle linear depolarization ratio (PLDR) in 1-K temperature bins. Shadings give the envelope of median curves for individual missions in PLDR high and PLDR low. Solid lines are averaged median curves. (b) Relative frequency of relative humidity over ice (RH_i) averaged over cases in PLDR high and PLDR low.

observe a difference in the supersaturated fraction of 11 percentage points and more is only 3.7%. This illustrates that the found raised PLDR distributions are linked to lower supersaturations in the clouds.

4. Discussion

The differences in PLDR and RH_i, found in our observations, raise the question what the responsible processes might be. PLDR is mainly determined by ice crystal shape, which is dependent on the temperature, supersaturation, and potentially the availability of ice nuclei during ice formation. The fact that we find specific cloud types like cirrus forming in the outflow of warm conveyor belts (M5, M10, and M14) or cirrus affected by embedded young contrails (M4, M7, M11, and M12) in both groups indicates that the large-scale meteorological situation and direct impacts from aviation are not the decisive factors in producing the differences in PLDR.

However, lower supersaturations in PLDR high cases could be a sign of more frequent heterogeneous freezing. For example, the presence of an additional type of ice nuclei would lead to freezing at its specific freezing threshold (Hoose & Möhler, 2012). This would deplete the available WV resulting in a smaller chance to reach supersaturations exceeding this threshold. As freezing at lower RHi is expected to influence ice habits (Bailey & Hallett, 2008; Schnaiter et al., 2016), this could influence the clouds PLDR. In addition, it cannot be ruled out that the shape of the ice nuclei and the location and distribution of nucleation sites on the aerosol particle could lead to preferred directions and geometries of ice growth.

As such findings have not been anticipated during the campaign planning and execution, unfortunately, no in situ measurements of the aerosol load at the location and time of cloud formation are available. Therefore, we resort to 24-hr backward trajectory calculations in order to learn more about possible sources of ice nuclei. One representative trajectory for every mission is plotted in Figure 3. The air masses stay at pressures between 230 and 380 hPa within the investigated time window. Trajectories from the Atlantic Ocean and the Iberian Peninsula (M4, M7, M8, M9, M11, M12, and M14) are higher in the atmosphere at pressures below 320 hPa. Those stemming from the Mediterranean Sea and North Africa show pressures above 300 hPa. Typical cruise altitudes of aircrafts over the North Atlantic lie at 29000 ft (315 hPa) and above. Over the mainland aviation emissions happen also at lower altitudes during ascent and descent from and to the airports.

The PLDR high clouds M4, M12, and M14 formed in a very busy air traffic corridor connecting Central Europe with North America. In contrast, air masses in the PLDR low cases M8 and M9 originate from a more southern part of the Atlantic Ocean. A comparison with the distribution of aircraft emissions (see Stettler et al., 2013) reveals substantially lower emissions in this area.

The trajectories for M7 and M11 look very similar at the first glance; however, M11 reaches its maximum IWC (star) already at the North African coast. Any emissions along the trajectory after that point might not influence the cloud, as no substantial further nucleation is expected. M7 reaches its maximum IWC over France, and its trajectory lies almost exactly along the air corridor from Central Europe to Madrid, the Canary
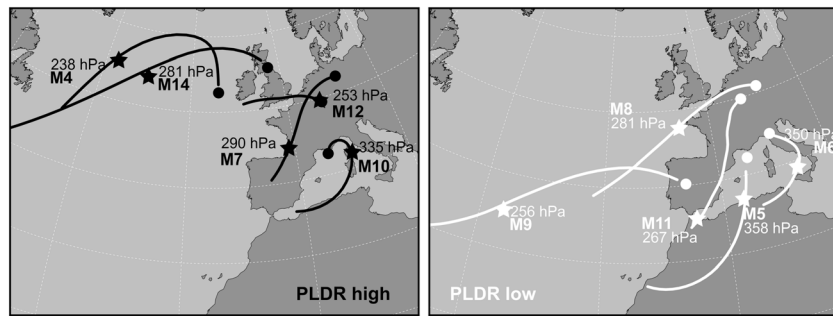
Figure 3. Location of measured cirrus clouds (dots), maximum cloud ice water content (stars), and the course of calculated backward trajectories for particle linear depolarization ratio (PLDR) high cases (black) and PLDR low cases (white).

Islands, and South America (see Stettler et al., 2013). Thus, the PLDR high case M7 might be affected by aviation emissions more heavily than the PLDR low case M11.

This co-occurrence of raised PLDR values and aviation emissions is less obvious for the cases M5, M6, and M10, as all three originate from the relatively "clean" region over the Mediterranean Sea and North Africa. Still the PLDR low cases stem from a more southern, and therefore, "cleaner" area and the PLDR high case reaches maximum IWC more closely to the European mainland in the more emission affected region of Northern Italy. This analysis shows that aviation cannot be excluded as the source of ice nuclei.

Besides the existence of ice nuclei, the small-scale dynamics of the air during ice nucleation is able to control microphysical parameters such as ice crystal number density and size (Kärcher, 2017). The updraft velocity influences temperature and relative humidity and could therefore indirectly impact the habit of forming ice crystals. As studies investigating the impact of vertical air motion concentrate mostly on ice number density and size, the influence on ice crystal shape however remains unclear.

5. Conclusions

During the ML-CIRRUS campaign 2014, cirrus clouds were measured by lidar over Europe with PLDR values that are on average 10 percentage points higher than in the other clouds. These altered optical properties come along with significantly lower supersaturations inside the clouds that may indicate more frequent heterogeneous freezing. A trajectory analysis revealed that the formation regions of the affected cirrus clouds lie in areas of high aviation emissions over the North Atlantic and the European mainland. Our investigations show that the possibility of an indirect aviation effect must not be neglected. Heterogeneous freezing on emitted exhaust particles could explain the lower supersaturations and higher PLDR that we found.

The aim of this work is to document the unexpected shift in PLDR and to raise attention to the possible influence of an indirect aviation effect. In our data, five out of 10 statistically independent cloud cases, measured during a period of 17 days, show elevated PLDR. The clouds dominated large areas over Europe at the time of their measurement. The fraction might be biased by the employed flight planning strategies, as three of the affected flights were dedicated to investigating contrail cirrus, and therefore, the flights took place in high air traffic regions. Nevertheless, in at least 29% of the days of the campaign this cloud type could be found over Europe.

The ML-CIRRUS research flights did not focus on indirect effects; therefore, crucial information at the cirrus formation regions was not explored in detail. For a deeper investigation, a mission strategy could include the characterization of the aerosol load in cirrus formation regions, the measurement of microphysical and optical properties of the emerging clouds, the measurement of the supersaturation and updraft velocity distribution during ice nucleation, and mission accompanying episodic modeling of aerosol and clouds that resolves daily and even diurnal changes in aviation emission patterns.

With this information, future flight campaigns can provide in-depth observational studies on the extent of the indirect aerosol effect on cirrus clouds.

References

Bailey, M., & Hallett, J. (2008). A comprehensive habit diagram for atmospheric ice crystals: Confirmation from laboratory, AIRS II and other field studies. *Journal of the Atmospheric Sciences*, *66*(9), 2888–2899. https://doi.org/10.1175/2009JAS2883.1

Burkhardt, U., & Kärcher, B. (2011). Global radiative forcing from contrail cirrus. *Nature Climate Change*, *1*(1), 54–58. https://doi.org/10.1038/nclimate1068

Burkhardt, U., Kärcher, B., & Schumann, U. (2010). Global modeling of the contrail and contrail cirrus climate impact. *Bulletin of the American Meteorological Society*, *91*(4), 479–484. https://doi.org/10.1175/2009BAMS2656.1

Del Guasta, M., Morandi, M., Stefanutti, L., Balestri, S., Kyro, E., Rummakainen, M., et al. (1998). Lidar observation of spherical particles in a −65° cold cirrus observed above Sodankyla (Finland) during S.E.S.A.M.E. *Journal of Aerosol Science*, *29*(3), 357–374. https://doi.org/10.1016/S0021-8502(97)10008-8

Del Guasta, M., & Vallar, E. (2003). In-cloud variability of LIDAR depolarization of polar and midlatitude cirrus. *Geophysical Research Letters*, *30*(11), 1578. https://doi.org/10.1029/2003GL017163

Esselborn, M., Wirth, M., Fix, A., Tesche, M., & Ehret, G. (2008). Airborne high spectral resolution lidar for measuring aerosol extinction and backscatter coefficients. *Applied Optics*, *47*(3), 346–358. https://doi.org/10.1364/AO.47.000346

Freudenthaler, V., Esselborn, M., Wiegner, M., Heese, B., Tesche, M., Ansmann, A., et al. (2009). Depolarization ratio profiling at several wavelengths in pure Saharan dust during SAMUM 2006. *Tellus B*, *61*(1), 165–179. https://doi.org/10.1111/j.1600-0889.2008.00396.x

Gettelman, A., & Chen, C. (2013). The climate impact of aviation aerosols. *Geophysical Research Letters*, *40*, 2785–2789. https://doi.org/10.1002/grl.50520

Groß, S., Wirth, M., Schäfler, A., Fix, A., Kaufmann, S., & Voigt, C. (2014). Potential of airborne lidar measurements for cirrus cloud studies. *Atmospheric Measurement Techniques*, *7*(8), 2745–2755. https://doi.org/10.5194/amt-7-2745-2015

Hendricks, J., Kärcher, B., Lohmann, U., & Ponater, M. (2005). Do aircraft black carbon emissions affect cirrus clouds on the global scale? *Geophysical Research Letters*, *32*, L12814. https://doi.org/10.1029/2005GL022740

Heymsfield, A., Baumgardner, D., DeMott, P., Forster, P., Gierens, K., & Kärcher, B. (2010). Contrail microphysics. *Bulletin of the American Meteorological Society*, *91*(4), 465–472. https://doi.org/10.1175/2009BAMS2839.1

Hoose, C., & Möhler, O. (2012). Heterogeneous ice nucleation on atmospheric aerosols: A review of results from laboratory experiments. *Atmospheric Chemistry and Physics*, *12*(20), 9817–9854. https://doi.org/10.5194/apc-12-9817-2012

Iwabuchi, H., Yang, P., Liou, K. N., & Minnis, P. (2012). Physical and optical properties of persistent contrails: Climatology and interpretation. *Journal of Geophysical Research*, *117*, D06215. https://doi.org/10.1029/2011JD017020

Jensen, E. J., & Toon, O. B. (1997). The potential impact of soot particles from aircraft exhaust on cirrus clouds. *Geophysical Research Letters*, *24*(3), 249–252. https://doi.org/10.1029/96GL03235

Kärcher, B. (2017). Cirrus clouds and their response to anthropogenic activities. *Current Climate Change Reports*, *3*(1), 45–57. https://doi.org/10.1007/s40641-017-0060-3

Kärcher, B., Burkhardt, U., Bier, A., Bock, L., & Ford, I. J. (2015). The microphysical pathway to contrail formation. *Journal of Geophysical Research: Atmospheres*, *120*, 7893–7927. https://doi.org/10.1002/2015JD023491

Kärcher, B., Möhler, O., DeMott, P. J., Pechtl, S., & Yu, F. (2007). Insights into the role of soot aerosols in cirrus cloud formation. *Atmospheric Chemistry and Physics*, *7*(16), 4203–4227. https://doi.org/10.5194/acp-7-4203-2007

Kristensson, A., Gayet, J.-F., Ström, J., & Auriol, F. (2000). In situ observations of a reduction in effective crystal diameter in cirrus clouds near flight corridors. *Geophysical Research Letters*, *27*(5), 681–684. https://doi.org/10.1029/1999GL010934

Lee, D., Fahey, D., Forster, P., Newton, P., Wit, R., Lim, L., et al. (2009). Aviation and global climate change in the 21st century. *Atmospheric Environment*, *43*(22-23), 3520–3537. https://doi.org/10.1060/j.atmosenv.2009.04.024

Lund, M. T., Aamaas, B., Berntsen, T., Bock, L., Burkhardt, U., Fuglestveldt, J. S., & Shine, K. P. (2017). Emission metrics for quantifying regional climate impacts of aviation. *Earth System Dynamics*, *8*(3), 547–563. https://doi.org/10.5194/esd-8-547-2017

McKenna, D. S., Konopka, P., Grooß, J. U., Günther, G., Müller, R., Spang, R., et al. (2002). A new chemical Lagrangian model of the stratosphere (CLaMS)—1. Formulation of advection and mixing. *Journal of Geophysical Research*, *107*(D16), 4309. https://doi.org/10.1029/2000JD000114

Murphy, D. M., & Koop, T. (2005). Review of the vapour pressure of ice and supercooled water for atmospheric applications. *Quarterly Journal of the Royal Meteorological Society*, *131*(608), 1539–1565. https://doi.org/10.1256/qj.04.94

Noel, V., Chepfer, H., Haeffelin, M., & Morille, Y. (2006). Classification of ice crystal shapes in midlatitude ice clouds from three years of Lidar observations over the SIRTA observatory. *Journal of the Atmospheric Sciences*, *63*(11), 2978–2991. https://doi.org/10.1175/JAS3767.1

Noel, V., Chepfer, H., Ledanois, G., Delaval, A., & Flamant, P. H. (2002). Classification of particle effective shape ratios in cirrus clouds based on the lidar depolarization ratio. *Applied Optics*, *41*(21), 4245–4257. https://doi.org/10.1364/AO.41.004245

Ovarlez, J., Gayet, J.-F., Gierens, K., Ström, J., Ovarlez, H., Auriol, F., et al. (2002). Water vapour measurements inside cirrus clouds in Northern and Southern Hemispheres during INCA. *Geophysical Research Letters*, *29*(16), 1813. https://doi.org/10.1029/2001GL014440

Sassen, K., & Benson, S. (2001). A Midlatitude cirrus cloud climatology from the facility for atmospheric remote sensing, Part II: Microphysical Properties Derived from Lidar Depolarization. *Journal of the Atmospheric Sciences*, *58*(15), 2103–2112. https://doi.org/10.1175/1520-0469(2001)058<2103:AMCCCF>2.0.CO;2

Sassen, K., & Zhu, J. (2009). A global survey of CALIPSO linear depolarization ratios in ice clouds: Initial findings. *Journal of Geophysical Research*, *114*, D00H07. https://doi.org/10.1029/2009JD012279

Schnaiter, M., Büttner, S., Möhler, O., Skrotzki, J., Vragel, M., & Wagner, R. (2012). Influence of particle size and shape on the backscatter linear depolarization ratio of small ice crystals—Cloud chamber measurements in the context of contrail and cirrus microphysics. *Atmospheric Chemistry and Physics*, *12*(21), 10,465–10,484. https://doi.org/10.5194/acp-12-10465-2012

Schnaiter, M., Järvinen, E., Vochezer, P., Abdelmonem, A., Wagner, R., Jourdan, O., et al. (2016). Cloud chamber experiments on the origin of ice crystal complexity in cirrus clouds. *Atmospheric Chemistry and Physics*, *16*(8), 5091–5110. https://doi.org/10.5194/acp-16-5091-2016

Schumann, U. (2012). A contrail cirrus prediction model. *Geoscientific Model Development*, *5*(3), 543–580. https://doi.org/10.5194/gmd-5-543-2012

Schumann, U., Baumann, R., Baumgardner, D., Bedka, S. T., Duda, D. P., Freudenthaler, V., et al. (2017). Properties of individual contrails: A compilation of observations and some comparisons. *Atmospheric Chemistry and Physics*, *17*(1), 403–438. https://doi.org/10.5194/acp-17-403-2017

Schumann, U., & Graf, K. (2013). Aviation-induced cirrus and radiative changes at diurnal timescales. *Journal of Geophysical Research: Atmospheres*, *118*, 2404–2421. https://doi.org/10.1002/jgrd.50184

Spichtinger, P., Gierens, K., Smit, H. G. J., Ovarlez, J., & Gayet, J.-F. (2004). On the distribution of relative humidity in cirrus clouds. *Atmospheric Chemistry and Physics*, *4*(3), 639–647. https://doi.org/10.5194/acp-4-639-2004

Stettler, M., Boies, A., Petzold, A., & Barrett, S. (2013). Global civil aviation black carbon emissions. *Environmental Science & Technology*, *47*, 10,397–10,404. https://doi.org/10.1021/es401356v

Ström, J., & Ohlsson, S. (1998). In situ measurements of enhanced crystal number densities in cirrus clouds caused by aircraft exhaust. *Journal of Geophysical Research*, *103*(D10), 11,355–11,361. https://doi.org/10.1029/98JD00807

Tesche, M., Achtert, P., Glantz, P., & Noone, K. J. (2016). Aviation effects on already-existing cirrus clouds. *Nature Communications*, *7*(1), 12016. https://doi.org/10.1038/ncomms12026

Um, J., McFarquhar, G. M., Hong, Y. P., Lee, S.-S., Jung, C. H., Lawson, R. P., & Mo, Q. (2015). Dimensions and aspect ratios of natural ice crystals. *Atmospheric Chemistry and Physics*, *15*(7), 3933–3956. https://doi.org/10.5194/acp-15-3933-2015

Voigt, C., Schumann, U., Jessberger, P., Jurkat, T., Petzold, A., Gayet, J.-F., et al. (2011). Extinction and optical depth of contrails. *Geophysical Research Letters*, *38*, L11806. https://doi.org/10.1029/2011GL047189

Voigt, C., Schumann, U., Minikin, A., Abdelmonem, A., Afchine, A., Borrmann, S., et al. (2017). ML-CIRRUS: The airborne experiment on natural cirrus and contrail cirrus with the high-altitude long-range research aircraft HALO. *Bulletin of the American Meteorological Society*, *98*(2), 271–288. https://doi.org/10.1175/BAMS-D-15-00213.1

Wirth, M., Fix, A., Mahnke, P., Schwarzer, H., Schrandt, F., & Ehret, G. (2009). The airborne multi-wavelength water vapor differential absorption lidar WALES: System design and performance. *Applied Physics B*, *96*(1), 201–213. https://doi.org/10.1007/s00340-009-3365-7

Zhou, C., & Penner, J. E. (2014). Aircraft soot indirect effect on large-scale cirrus clouds: Is the indirect forcing by aircraft soot positive or negative? *Journal of Geophysical Research: Atmospheres*, *119*, 10,981–10,995. https://doi.org/10.1002/2014JD021924